ACS OMEGA

http://pubs.acs.org/journal/acsodf

Article

Microorganisms@*a*MIL-125 (Ti): An Amorphous Metal−Organic Framework Induced by Microorganisms and Their Applications

Yuqiang Xiang, Huaduo Yan, Fei Peng, Weikang Ke, Aroosha Faheem, Mingshun Li,* and Yonggang Hu*

Cite This: *ACS Omega* 2023, 8, 2164−2172

Read Online

ACCESS | Metrics & More | Article Recommendations | Supporting Information

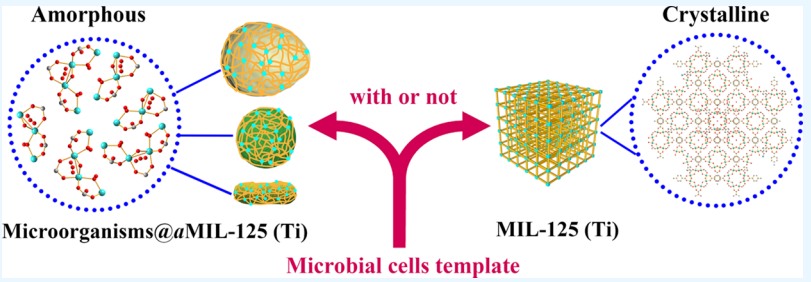

ABSTRACT: Amorphous metal−organic framework (*a*MOF)-based materials have attracted considerable attention as an emerging class of nanomaterials. Herein, novel microorganisms@*a*MIL-125 (Ti) composites including yeast@*a*MIL-125 (Ti), PCC 6803@*a*MIL-125 (Ti), and *Escherichia coli*@*a*MIL-125 (Ti) composites were respectively synthesized by self-assembling *a*MOFs on the microorganisms' surface. The functional groups on the microorganisms' surface induced structural defects and participated in the formation of *a*MIL-125 (Ti) composites. Finally, the application of microorganisms@*a*MIL-125 (Ti) composites for the removal of glyphosate from aqueous solution was selected as a model reaction to illustrate their potential for environmental protection. The present method is not only economical but also has other advantages including ease of operation, environmentally friendly assay, and high adsorption. The maximum adsorption capacity of *a*MIL-125 (Ti) was 1096.25 mg g^{-1}, which was 1.74 times that of crystalline MIL-125 (Ti). Therefore, the microorganisms@*a*MOFs composites will have broad application prospects in energy storage, drug delivery, catalysis, adsorbing toxic substances, sensing, encapsulating and delivering enzymes, and in other fields.

1. INTRODUCTION

Recently, scientific interest in amorphous metal−organic frameworks (*a*MOFs) with metal−ligand bonding motifs similar to their crystalline counterparts is rising. *a*MOFs are networks of inorganic nodes (metal ions or clusters) connected by organic ligands in either two or three dimensions with potential for porosity and display no long-range periodic order within the structure. *a*MOFs, owing to their excellent physical and chemical properties, such as high conductivity, rich active metal sites, hierarchical porosity, improved mass transport,[1,2] and significantly different guest species adsorption and release behaviors due to the partial collapse of the porous MOF frameworks,[3] have gradually caught attention in multiple areas such as energy storage,[4] drug delivery,[5] catalysis,[6,7] adsorbing toxic substances,[8,9] sensing,[10] encapsulating and delivering enzymes,[11] and so on. The existing *a*MOFs were prepared via amorphization of crystalline MOFs by the electron-beam-induced method,[12] high pressure,[13−16] high-energy ball milling,[17,18] high-temperature heating,[6,19,20] and chemical treatment.[4,7,21] However, these methods suffered some problems such as multiple preparation steps, being time-consuming, and sophisticated synthesis conditions. To date, the reported *a*MOFs account for only a small fraction of mesoporous porous materials (less than 200) and much lower than that of crystalline MOFs (over 99,000).[9,22] A new synthetic method to prepare *a*MOFs is therefore highly desired.

Microorganisms are a type of bioresource material that can be mass produced by fermentation. The use of microorganisms to prepare functional materials offers various benefits such as low cost, fast productivity, biomineralization ability, and environmental friendliness.[23−27] For example, several nanoparticles including AuNPs, Fe_3O_4, TiO_2, and Fe^0 have been assembled onto microorganisms to form composites, which exhibited attractive application prospects in scientifically and technologically important areas including biosensing, tumor therapy, catalysis, and pollutant treatment.[23,28−30] Recently, we

Received: September 30, 2022
Accepted: December 14, 2022
Published: January 4, 2023

https://doi.org/10.1021/acsomega.2c06329
ACS Omega 2023, 8, 2164−2172

presented the use of microorganisms in the preparation of microorganism@MOFs composites, which have been successfully used for sensing and adsorbing harmful substances.[24−26] Interestingly, we found that the functional groups on the surface of microorganisms can induce structural defects in some MOFs (such as UiO-66-Zr, UiO-67-Zr, and ZIF-8). Furthermore, we accidentally found that the existence of microorganisms could cause the crystal structure of MIL-125 (Ti, MIL = Materials of Institute Lavoisier) to completely disappear and get an amorphous product. Inspired by the above findings, we presented a simple and versatile bottom-up method for the preparation of *a*MIL-125 (Ti) by assembling MIL-125 (Ti) on the microorganisms' surface (Scheme 1).

Scheme 1. Schematic Representation of the Synthesis of the *a*MIL-125 (Ti) Membranes Induced by Microbial Cell-Based Templates

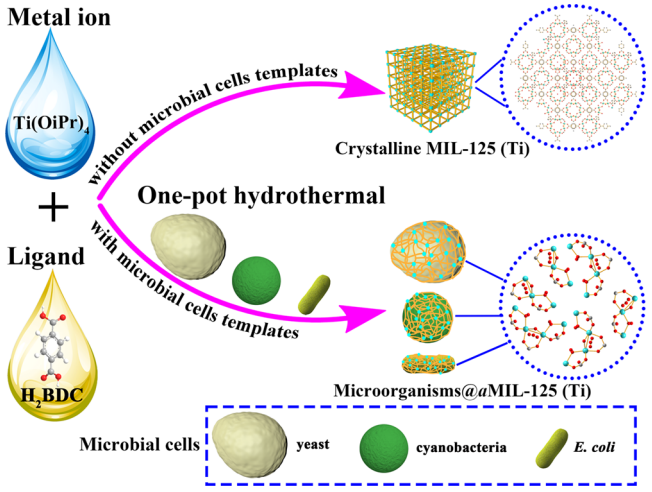

The metal ion and ligand of synthesized MIL-125 (Ti) and three types of nonpathogenic microorganisms, including *Saccharomyces cerevisiae* (baker's yeast), *Synechocystis* sp. PCC 6803 (PCC 6803), and *Escherichia coli* DH5*α* (*E. coli*), were used to validate this hypothesis and to form novel *a*MIL-125 (Ti)-based composites. The formation mechanism of microorganisms@*a*MIL-125 (Ti) was then investigated with a series of characterization techniques. Finally, microorganisms@*a*MIL-125 (Ti) were used to remove the glyphosate from aqueous solution, demonstrating potential application prospects of microorganisms@*a*MIL-125 (Ti). The adsorption behavior and mechanism of yeast@*a*MIL-125 (Ti) composites for glyphosate were also explored in detail. Hence, this work will provide a new strategy for the preparation of advanced *a*MOF materials with various features, as well as guidelines for the design of *a*MOF nanomaterials.

2. EXPERIMENTAL SECTION

2.1. Chemicals and Materials. Terephthalic acid (H_2BDC), glyphosate (99%), potassium bromide (KBr, 99.95%), and sodium nitrite ($NaNO_2$, 99.999%) were purchased from Sigma-Aldrich Trading Co., Ltd. (Shanghai, China). Titanium(IV) isopropoxide [$Ti(OiPr)_4$, 99.995%] was purchased from Alfa Aesar (Shanghai, China). *N*,*N*-Dimethylformamide (DMF), methanol (99.7%), ethanol, and sulfuric acid (H_2SO_4, 96.0%) were purchased from Sinopharm Chemical Reagent Co., Ltd. (China). *S. cerevisiae*, PCC 6803, and *E. coli* (*DH5α*) strains were kindly provided by State Key Laboratory of Agricultural Microbiology, Huazhong Agricultural University. Ultrapure water (18.2 MΩ·cm) collected from a laboratory ultrapure water purification system (model Cascada I, Pall Co., Ltd., Washington, NY, USA) was used to prepare all the solutions.

2.2. Cultivation of Microorganisms. The microorganisms (yeast, PCC 6803 and *E. coli*) were cultured by following our previous method.[24] These microorganisms were collected by centrifugation after being cultured for the appropriate time, then washed with ultrapure water three times to remove free medium, resuspended in 10% formaldehyde, and stored at 4 °C for further usage.

2.3. Synthesis of Microorganisms@*a*MIL-125 (Ti) Composites and MIL-125 (Ti). Microorganisms@*a*MIL-125 (Ti) composites were synthesized by a one-pot hydrothermal method with slight modification.[31] In short, H_2BDC (0.12 g) was dispersed in 9 mL of DMF and 1 mL of methanol in a Teflon-lined autoclave at 25 °C for 5 min, and then the microorganisms' pellets (yeast, PCC 6803 or *E. coli* pellets, 1 g, wet weight) were resuspended in 5 mL of DMF and mixed with the above solution. Afterward, 200 *μ*L of $Ti(OiPr)_4$ was introduced to the above mixture. Finally, the mixture was heated for few minutes and kept at 150 °C for 24 h. The obtained white solid was thoroughly washed with DMF and ethanol three times and then dried in an oven at 100 °C for 12 h. The MIL-125 (Ti) was synthesized using the same protocol without adding microorganism cells.

2.4. Characterization. Phase-contrast micrographs were obtained using an Olympus BX51 microscope (Olympus Corp., Japan). Field-emission scanning electron microscopy (FE-SEM) images were obtained using an electron microscope (SU-8010, Hitachi, Ltd., Tokyo, Japan) equipped with energy-dispersive spectroscopy (EDS). Zeta potential was measured on a Malvern Zetasizer Nano analyzer (Malvern, ZEN 3600). Wide-angle powder X-ray diffraction (PXRD) measurements were performed using an X-ray diffractometer (D/MAX-RB, Rigaku, Tokyo, Japan) with Cu K*α* radiation (λ = 1.54056 Å) over the 2θ range of 5−50°. N_2 adsorption−desorption isotherms were recorded using a Micromeritics ASAP 2460 sorptometer (Atlanta, USA) at 77 K. The specific surface areas were calculated using the Brunauer−Emmett−Teller method. The pore size distributions were derived from the adsorption branches of isotherms using the Barrett−Joyner−Halenda method. Fourier transform infrared (FTIR) spectra were obtained using a FTIR spectrophotometer (Vertex 70, Bruker Optics, Ettlingen, Germany) within the 400−4000 cm^{-1} region. X-ray photoelectron spectroscopy (XPS) was performed using a VG Multilab 2000 (Thermo Fisher Scientific, Waltham, MA, USA) spectrometer with monochromatic Al K*α* radiation. Binding energy values were charge-corrected to the adventitious carbon (C 1s = 284.8 eV). The ultraviolet visible (UV−vis) spectra were recorded using a UV-2600 spectrophotometer (Shimadzu, Japan).

2.5. Adsorption Experiments. Glyphosate adsorption experiment studies were performed in a batch at 25 °C, and the details of the adsorption experiment are described in the Supporting Information.

2.6. Statistics and Data Analysis. The data fit of the adsorption model was performed using Origin (version OriginPro 2020 Learning Edition, OriginLab Co., USA).

https://doi.org/10.1021/acsomega.2c06329
ACS Omega 2023, 8, 2164−2172

3. RESULTS AND DISCUSSION

3.1. Synthesis and Characterization of Microorganisms@*a*MIL-125 (Ti) Composites. First, microbial cells including yeast, PCC 6803, and *E. coli* were respectively treated and inactivated by using formaldehyde to avoid collapse or breakage during subsequent application and storage.[23,24] The inactivated microorganism cells (yeast, PCC 6803 and *E. coli*), MIL-125 (Ti), and microorganism@*a*MIL-125 (Ti) composites were then characterized by using phase-contrast microscopy, FE-SEM, zeta potential, PXRD, and nitrogen adsorption−desorption isotherms measurement, respectively. The phase-contrast microscopy images (Figure S1, Supporting Information) showed that the as-prepared microorganisms@*a*MIL-125 (Ti) composites had good uniformity and monodispersity similar to that of the inactivated yeast, PCC 6803, and *E. coli* cells. The surface of microorganisms@*a*MIL-125 (Ti) composites had a thin coating of nanoparticles (Figure 1a_2,b_2,c_2), compared to the smooth

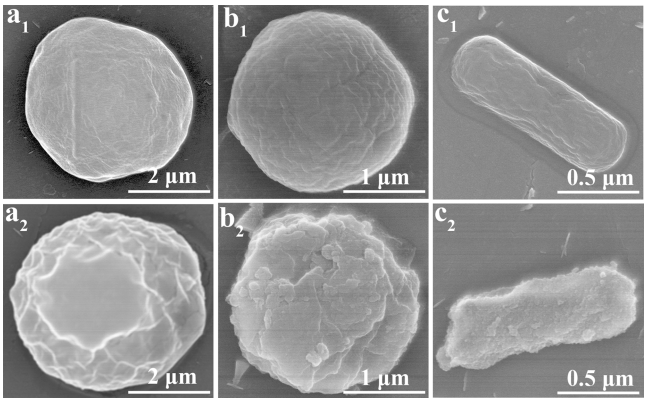

Figure 1. FE-SEM images of microorganisms and microorganisms@*a*MIL-125 (Ti) composites. (a_1) yeast, (a_2) yeast@*a*MIL-125 (Ti), (b_1) PCC 6803, (b_2) PCC 6803@*a*MIL-125 (Ti), (c_1) *E. coli*, and (c_2) *E. coli*@*a*MIL-125 (Ti).

surface of pristine yeast, PCC 6803, and *E. coli* cells (Figure 1a_1,b_1,c_1). The morphology of the nanoparticles on the surface of microorganisms was quite different from that of the as-prepared MIL-125 (Ti) (Figure S2, Supporting Information). After the formation of microorganisms@*a*MIL-125 (Ti) composites, the zeta potential values of yeast (−42.3 mV), PCC 6803 (−26.1 mV), and *E. coli* (−46.6 mV) were changed to −2.5, 4.4, and −8.6 mV, respectively (Figure S3, Supporting Information), indicating the presence of a Ti-based nanoparticle on the surface of microorganisms.

As shown in Figure 2a−c and Table S1 (Supporting Information), the average pore size of yeast@*a*MIL-125 (Ti), PCC 6803@*a*MIL-125 (Ti), and *E. coli*@*a*MIL-125 (Ti) composites was 3.90, 4.05, and 4.53 nm, respectively. The corresponding value for MIL-125 (Ti) was 2.65 nm (Figure 2d and Table S1, Supporting Information), which agreed with that reported previously (2.40 nm).[31] Obviously, the average pore sizes of composites increased by about 1.6 times in comparison with that of crystalline MIL-125 (Ti). This finding revealed that Ti-based nanoparticles on the surface of microorganisms were a new mesoporous material but not crystalline MIL-125 (Ti).

As shown in Figure 3, the PXRD patterns of microorganisms@*a*MIL-125 (Ti) composites absolutely mismatched with the simulated patterns of the MIL-125 (Ti), while the as-prepared MIL-125 (Ti) had high crystallinity and its diffraction peak could be perfectly matched with the simulated PXRD pattern. When the microorganism pellets were added into the reaction system, the most prominent feature of the PXRD patterns of composites was the appearance of a new strong and broad asymmetric "hump" at approximately 19°, while most of the main characteristic peaks of the simulated patterns disappeared in the composites' patterns, suggesting the presence of a highly amorphous structure in these composites.[32] Accordingly, the results of PXRD combined with that characterized by SEM, zeta potential, and nitrogen adsorption−desorption isotherms measurement showed that the Ti-based nanomaterial coated on the yeast cell surface was a new kind of *a*MOF with a mesoporous structure.

The yeast@*a*MIL-125 (Ti) composites as a model were further characterized by using EDS, FTIR, and XPS techniques. The EDS mappings clearly showed the presence of homogeneously and continuously distributed Ti, C, O, N, and P elements and an overlayer of the above elements in yeast@*a*MIL-125 (Ti) (Figure 4), indicating that the *a*MIL-125 (Ti) film was uniformly coated on the surface of the yeast cell. As shown in Figure S4 (Supporting Information), it can be confirmed that the presence of −COOH (3363 and 1656 cm^{-1}), amide I (1656 cm^{-1}), amide II (1544 cm^{-1}), −OH (3363, 2925, 1385 and 1044 cm^{-1}), and $-PO_3$ groups (1242 and 1044 cm^{-1}) on the yeast cell wall will provide a wide range of fixed sites to stabilize various metals.[23,24,33] The characteristic peak at 1049 cm^{-1} indicated the formation of Ti−O−C═O or Ti−O−C between the Ti precursor and functional groups (e.g., −COOH, −OH, amide and $-PO_3$) present on the surface of yeast cells.[34] The wavenumbers red-shifts of 18 cm^{-1} at 3363 cm^{-1}, 7 cm^{-1} at 2925 cm^{-1}, 3 cm^{-1} at 1242 cm^{-1}, and 5 cm^{-1} at 1044 cm^{-1} were observed, while the wavenumbers blue-shift of 7 cm^{-1} at 1656 cm^{-1}, and 6 cm^{-1} at 1544 cm^{-1} were observed after the formation of yeast@*a*MIL-125 (Ti) composites. Additionally, the free yeast's FTIR spectrum showed that the asymmetric stretching vibration (−COOH) signal is apparent at about 1656 cm^{-1}, which was different from the coordinated asymmetric stretching vibration at 1649 cm^{-1} for yeast@*a*MIL-125 (Ti).[35] Such a difference suggests the successful coordination between −COOH groups from yeast and Ti ions. These observations could be ascribed to the stretching vibration of C═O, C−O, C−N, O−H, N−H, and P−O bonds. The shifted FTIR signals of −COOH, −OH, amide I, amide II, and $-PO_3$ groups suggested that these functional groups present on the surface of yeast cells may be involved in inducing the amorphization of the MIL-125 (Ti).

The survey XPS spectrum of yeast@*a*MIL-125 (Ti) composites exhibited the characteristic spectra of Ti 2p (Figure S5a, Supporting Information). The Ti 2p spectrum of yeast@*a*MIL-125 (Ti) composites showed two main peaks located at 457.07 and 462.78 eV (Figure S5b, Supporting Information), which were attributed to Ti $2p_{3/2}$ and Ti $2p_{1/2}$, respectively.[36] In addition, the high-resolution XPS spectra of C 1s for yeast cells (Figure S5c, Supporting Information) can be divided into three different peaks at 284.54, 285.92, and 287.39 eV, corresponding to C−C/C−H, carboxylate group (O−C═O), and carbonyl group (C═O) bonds, respectively.[24] As shown in Figure S5d (Supporting Information), the O 1s spectra of yeast cells present the bonds of −OH and C−O/C═O at 531.85 and 532.45 eV, respectively.[33] The N 1s spectra of yeast cells showed the amide centered at 399.56 eV

https://doi.org/10.1021/acsomega.2c06329
ACS Omega 2023, 8, 2164−2172

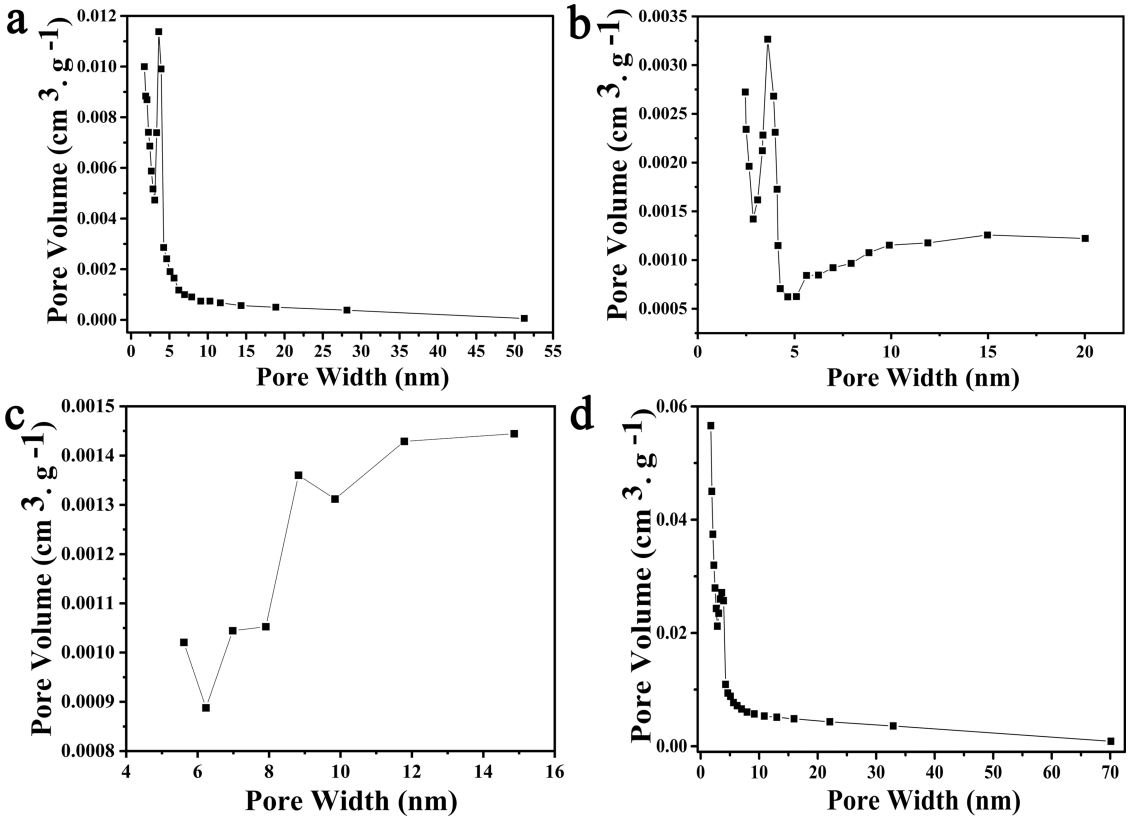

Figure 2. Pore size distributions of (a) yeast@*a*MIL-125 (Ti), (b) PCC 6803@*a*MIL-125 (Ti), (c) *E. coli*@*a*MIL-125 (Ti), and (d) MIL-125 (Ti).

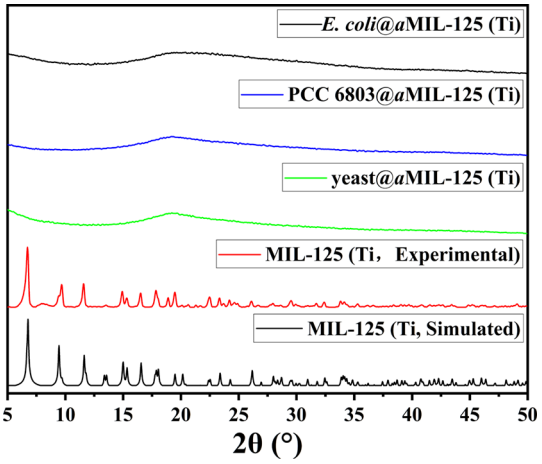

Figure 3. Simulated and experimental PXRD patterns of MIL-125 (Ti) and microorganisms@*a*MIL-125 (Ti) composites.

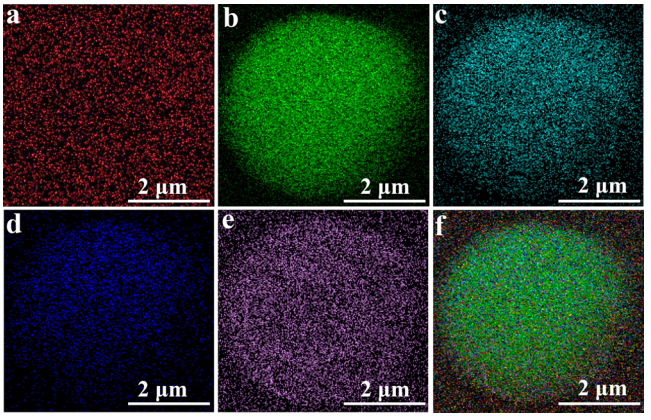

Figure 4. EDS characterization of yeast@*a*MIL-125 (Ti) composites. EDS element mappings of (a) Ti, (b) C, (c) O, (d) N, (e) P, and (f) overlayer of the above elements of yeast@*a*MIL-125 (Ti) composites, respectively.

while protonated amine at 400.35 eV (Figure S5e, Supporting Information), respectively.[37] Moreover, as shown in Figure S5f (Supporting Information), the P 2p high-resolution XPS spectra of yeast cells can be deconvoluted into two peaks at 133.06 eV (P−O) and 134.07 eV (C−O−P),[38,39] which confirms the presence of $-PO_3$ on the surface of yeast cells. After the formation of yeast@*a*MIL-125 (Ti) composites, it could be clearly observed that the peaks at 283.2, 528.94, 531.11, 400.35, 132.06, and 133.31 eV were attributed to C−Ti−O,[40] lattice oxygen (O^{2-}),[34] Ti−OH,[33,41] N−C═O,[42] P−C, and P−O bonds,[38] respectively, suggesting no characteristic binding energy of Ti−N (456.4 eV) and Ti−P bonds (455.40 eV).[43] Notably, the binding energies and atomic proportions (atom %) of C 1s, O 1s, N 1s, and P 2p in −COOH, −OH, amide and $-PO_3$ groups have significantly changed after the formation of yeast@*a*MIL-125 (Ti) composites (Figure S5c−f, Supporting Information). The apparent changes in composition are most likely caused by changes in the structure of the material.[6] Combined with the results of FTIR, we believe that the functional groups including −COOH, −OH, amide, and $-PO_3$ on the surface of yeast cells were coordinately competed with the Ti-oxo cluster and formed the intermolecular hydrogen bond between the functional groups of −COOH, −OH, and $-NH_2$ in yeast cells with the organic linkers (H_2BDC) during the stirring process.[44] Such coordination interactions lead to the defects in the crystal structure of MIL-

https://doi.org/10.1021/acsomega.2c06329
ACS Omega 2023, 8, 2164−2172

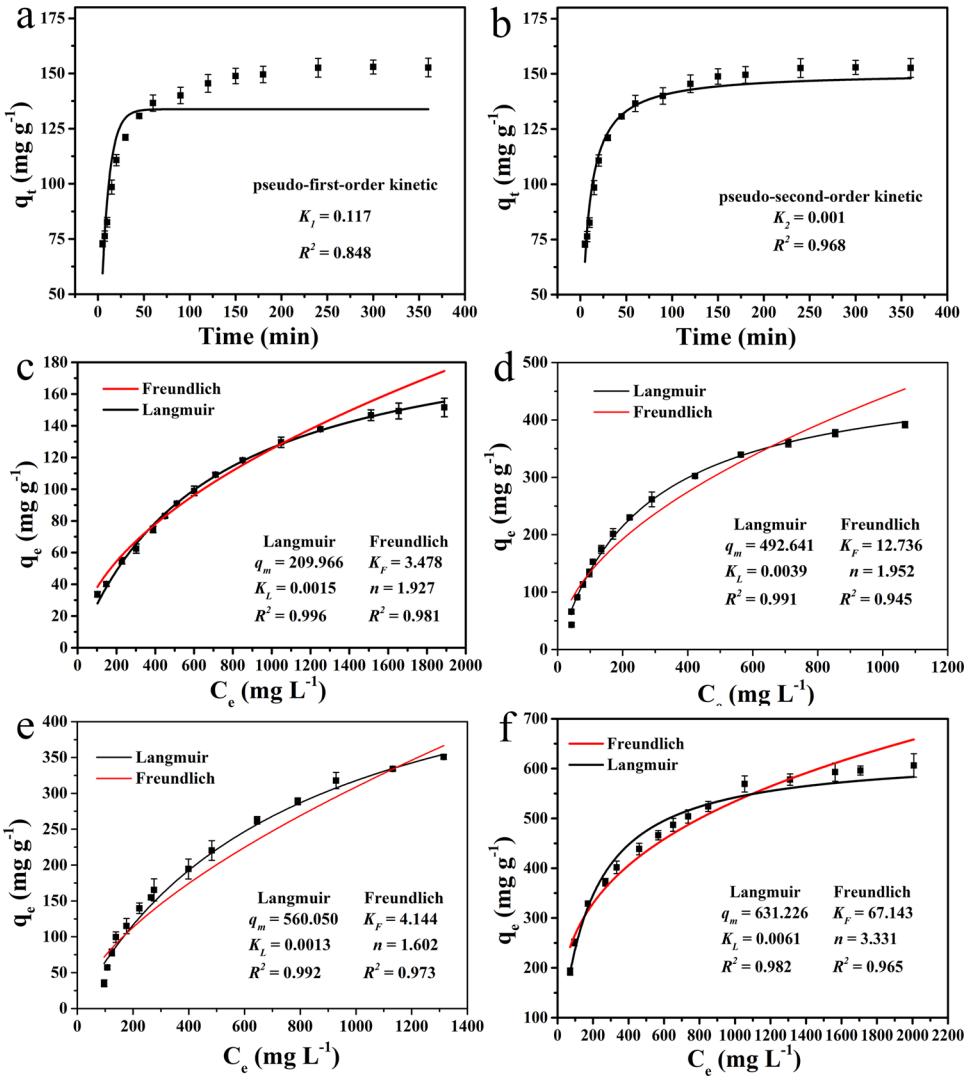

Figure 5. Adsorption performance of glyphosate by microorganisms@*a*MIL-125 (Ti) composites and crystalline MIL-125 (Ti). Adsorption kinetics and nonlinear fitting curves of glyphosate on yeast@*a*MIL-125 (Ti) composites using (a) pseudo-first-order and (b) pseudo-second-order kinetic models. Reaction conditions: glyphosate concentration: 1.0 mg mL^{-1}; adsorbent dosage: 3.75 mg (dry weight); pH 3.0; temperature: 25 °C. Langmuir and Freundlich isotherms model curves of (c) yeast@*a*MIL-125 (Ti) composites, (d) PCC 6803@*a*MIL-125 (Ti) composites, (e) *E. coli*@*a*MIL-125 (Ti) composites, and (f) crystalline MIL-125 (Ti) toward glyphosate, where q_m (mg g^{-1}) is the theoretical maximal adsorption capacities of adsorbent, C_e is the glyphosate concentration after equilibrium was reached, K_L (L mg^{-1}) is the Langmuir adsorption constant, K_F (L mg^{-1}) is the Freundlich adsorption constant related to the adsorption capability of the adsorbent, and n is the heterogeneity factor. Reaction conditions: initial glyphosate concentration: 0.2 to 2.5 mg mL^{-1}; adsorbent dosage: 3.75 mg (dry weight); pH 3.0; reaction time: 240 min; temperature: 25 °C.

125 (Ti) resulting from disordered links between metal ions and organic ligands.[45] That is, functional groups on the surface of the microbial cell wall could alter the energy barriers of MOF nucleation, promote crystal growth pathway, and lead to an entropy-driven process (i.e., amorphization) to form microorganism@*a*MIL-125 (Ti) composites.[1,7,46] Obviously, this developed method is quite different from the conventional methods, providing a cost-effective and convenient way to prepare new *a*MOF-based materials under mild conditions.

3.2. Adsorption of Glyphosate on Microorganisms@*a*MIL-125 (Ti) Composites. Glyphosate is the most widely used broad-spectrum herbicide derived from glycine in the world.[47] The extensive use of glyphosate has caused widespread environmental pollution and has potential links with human cancer and other chronic diseases.[48−50] Therefore, exploring effective adsorbents to remove glyphosate from the environment is highly desired. The use of microorganisms@*a*MIL-125 (Ti) composites as a new adsorbent for glyphosate removal was investigated in the subsequent experiments, and the yeast@aMIL-125 (Ti) composite was selected as an example. As shown in Figure S6a (Supporting Information), the effect of pH on glyphosate adsorption was investigated by varying from 1.0 to 10.0. The glyphosate adsorption capacity of the yeast@*a*MIL-125 (Ti) composite increased from 1.0 to 3.0 and decreased with the continuous increase in pH reaching above 3.0. The zeta potential value of yeast@*a*MIL-125 (Ti) composites decreased from −2.51 to −5.89 mV after glyphosate adsorption at pH 3.0 (Figure S6b, Supporting Information), because glyphosate becomes electronegative when pH increased to 3.0 and even more.[51−53] Results in Figure S6c (Supporting Information) revealed that the surface potential of yeast@*a*MIL-125 (Ti) composites was a negative

https://doi.org/10.1021/acsomega.2c06329
ACS Omega 2023, 8, 2164−2172

value above pH 3.0. Accordingly, the electrostatic attraction was not the main factor of glyphosate adsorption on the yeast@*a*MIL-125 (Ti) composite surface.

The adsorption of glyphosate was further investigated using FTIR and XPS, respectively. As shown in Figure S7a (Supporting Information), several characteristic peaks were red-shifted after the adsorption of glyphosate, including −COOH (3381 and 1649 cm^{-1}) and −OH (3381 and 1386 cm^{-1}), indicating that the intermolecular hydrogen bonding could be formed between the −COOH and −OH groups of organic linkers (H_2BDC) and the −COOH, −NH−, and $-H_2PO_3$ groups present in glyphosate.[54] As shown in Figure S7b−d (Supporting Information), the binding energies and atom% of C 1s, O 1s and Ti 2p peaks of yeast@*a*MIL-125 (Ti) composites before and after the adsorption of glyphosate were not significantly changed. Compared with the N 1s and P 2p spectra of yeast@*a*MIL-125 (Ti) composites (Figure S7e−f, Supporting Information), the binding energies and atom% of N 1s and P 2p were obviously changed after glyphosate adsorption, indicating that the electron density in the N and P atoms of glyphosate was either lost or accepted electrons.[55] Combined with the results shown in FTIR, the XPS data revealed the adsorption of glyphosate by yeast@*a*MIL-125 (Ti) composites is a chemisorption process. This process was attributed to the affinity between the titanium-based active centers in the yeast@*a*MIL-125 (Ti) composites, the phosphate group, and the amino groups present in the glyphosate molecule.[56] Given the concentration of OH^-, which increased with the increase of pH above 3.0 (Figure S6a, Supporting Information), the gradual decrease of glyphosate adsorption capacity of the yeast@*a*MIL-125 (Ti) composite might be due to the presence of competitive reactions between glyphosate and OH^-.

The adsorption kinetics of yeast@*a*MIL-125 (Ti) composites were evaluated in a glyphosate solution (the concentration from 0.2 to 2.5 mg mL^{-1}). As shown in Figure 5a,b, the pseudo-first-order and pseudo-second-order models were used to analyze the way of the adsorption interaction, indicating that the pseudo-second-order model was more appropriate in describing the adsorption process with a higher R^2 value. Additionally, the data fitted well with the pseudo-second-order model, suggesting that the adsorption rate depends on the concentration of function sites of yeast@*a*MIL-125 (Ti) composites.[56−59] The specific surface area and total pore volume of the yeast@*a*MIL-125 (Ti) composites after adsorption of glyphosate molecules were smaller than those before adsorption (Figure S8 and Table S1, Supporting Information), which confirmed that glyphosate molecules were adsorbed into the pore cavities of yeast@*a*MIL-125 (Ti) composites. The adsorption capacity of yeast@*a*MIL-125 (Ti) composites for glyphosate increased rapidly in the first 60 min and reached equilibrium within 240 min. The reason might be the presence of plenty of vacant binding sites on the surface of yeast@*a*MIL-125 (Ti) composites during the initial 60 min, which were favorable for rapid adsorption of glyphosate. Subsequently, the adsorbent cavities were gradually and partially blocked by the absorbed glyphosate molecules, preventing other glyphosate molecules from combining with the adsorption sites on the adsorbents,[56,57,60] resulting in a gradual decrease in the adsorption rate and finally reaching equilibrium after 240 min.

As shown in Figure 5c−e, the adsorption isotherms of glyphosate on microorganisms@*a*MIL-125 (Ti) composites were more consistent with the Langmuir model, which showed better fit than the Freundlich model with higher R^2 values, suggesting that the adsorption process may be monolayer adsorption. Therefore, the adsorption process of glyphosate on microorganisms@*a*MIL-125 (Ti) composites could be ascribed to a homogeneous and monolayer adsorption.[61] According to the Langmuir isotherm model, the maximum adsorption capacity (q_m) of glyphosate on yeast@*a*MIL-125 (Ti), PCC 6803@*a*MIL-125 (Ti), and *E. coli*@*a*MIL-125 (Ti) composites was 209.966, 492.641, and 560.050 mg g^{-1}, respectively. We noticed that the proportion of *a*MOFs in the yeast@*a*MIL-125 (Ti), PCC 6803@*a*MIL-125 (Ti), *and E. coli*@*a*MIL-125 (Ti) composites was 19.4, 44.9, and 50.5%, respectively. Meanwhile, no significant adsorption of glyphosate on the microbial surface was observed during our experiments (Figure S9, Supporting Information). Obviously, the adsorption of glyphosate composites was due to the formation of *a*MOFs on the surface of microorganisms, and the different q_m was due to the proportion of the *a*MOF with a similar structure and aperture in yeast@*a*MIL-125 (Ti), PCC 6803@*a*MIL-125 (Ti), and *E. coli*@*a*MIL-125 (Ti) composites. The q_m of *a*MIL-125 (Ti) after removing the weight of microbial cells was then calculated. As shown in Table 1, q_m of *a*MIL-125 (Ti) obtained from yeast@*a*MIL-125 (Ti), PCC 6803@*a*MIL-125 (Ti), and *E. coli*@*a*MIL-125 (Ti) composites was 1082.45, 1097.19, and 1109.00 mg g^{-1}, respectively. That is, the *a*MOF obtained on different microbial surfaces with the same amount of MOF raw materials had a similar structure and properties. Hence, the same adsorption effect can be obtained after removing the microbial weight. The q_m of *a*MIL-125 (Ti) was about 1.7 times that of crystalline MIL-125 (Ti) (631.226 mg g^{-1}, Figure 5f), which was better than that of the other reported adsorbents listed in Table 1. As shown in Figure 2 and Table S1 (Supporting Information), the aperture of *a*MIL-125 (Ti) was obviously larger than that of crystalline MIL-125 (Ti). However, the specific surface area and total pore volume of *a*MOFs were smaller than those of the MOF. Given this perspective, the increase of the pore size of *a*MOFs is the key factor for the increase of glyphosate q_m, because the large pore size and structural defects of *a*MOFs could effectively improve mass transport and active molecular metal sites.[9,62]

Table 1. Comparison of the Adsorption Capacities of Glyphosate by Various Adsorbents

adsorbents	q_{max} (mg g^{-1})	references
Kaolinite-humic acid composites	0.996	55
aminated lignin/Fe_3O_4/$La(OH)_3$	83.87	63
Cu-zeolite 4A	112.7	64
$MnFe_2O_4$−graphene	39	52
$MnFe_2O_4$@activated carbon	167.2	65
UiO-67	537	56
Fe_3O_4@SiO_2@UiO-67	256.54	60
UiO-67/graphene	482.69	57
NH_2-MIL-101 (Cr)	64.25	66
MIL-101 (Fe)	107.70	67
NH_2-MIL-101(Fe)	124.38	67
Fe_3O_4@NH_2-MIL-101(Fe)	11.95	68
*a*MIL-125 (Ti)$_{(Yeast)}$	1082.45	this work
*a*MIL-125 (Ti)$_{(PCC\ 6803)}$	1097.19	this work
*a*MIL-125 (Ti)$_{(E.\ coli)}$	1109.00	this work
MIL-125 (Ti)	631.226	this work

https://doi.org/10.1021/acsomega.2c06329
ACS Omega 2023, 8, 2164−2172

As shown in Figure S10 (Supporting Information), the effect of coexisting cations on the adsorption of glyphosate by yeast@*a*MIL-125 (Ti) composites was also investigated with different concentrations (5 and 50 mM) of Na^+, K^+, Mg^{2+}, Ca^{2+}, and Al^{3+}. The almost unchanged adsorption capacities of glyphosate indicate that the effect on the adsorption of glyphosate caused by these coexisting metal ions could be negligible under tested conditions. Moreover, as shown in Figure S11 (Supporting Information), the adsorption efficiency of the three microorganisms@*a*MIL-125 (Ti) composites can retain above 70% after five cycles, indicating that the as-prepared microorganisms@*a*MIL-125 (Ti) composites can be used to remove glyphosate from polluted water for at least five times. Hence, microorganisms@*a*MIL-125 (Ti) composites proved to be a prospective glyphosate adsorbent with high application potential.

4. CONCLUSIONS

In summary, we have developed a facile, straightforward, low-cost, and environmentally friendly strategy to induce amorphization of MIL-125 (Ti) through functional groups on the surface of microorganisms. The formation of microorganisms@*a*MIL-125 (Ti) composites was a chemical self-assembly process. The as-prepared microorganisms@*a*MIL-125 (Ti) composites exhibited high adsorption capacity toward glyphosate, attributed to the adequate pore size and strong affinity between the low-coordinated titanium-based active centers in the microorganism@aMIL-125 (Ti) composites and glyphosate. This work has provided an innovative amorphization strategy for the synthesis of novel *a*MOF-based composites with enhanced performance, which can be extensively employed in gas adsorption, pollutant treatment, drug delivery, and biosensing.

■ ASSOCIATED CONTENT

Supporting Information

The Supporting Information is available free of charge at https://pubs.acs.org/doi/10.1021/acsomega.2c06329.

Adsorption experiments, reusability of microorganisms@aMIL-125 (Ti) composites and sample analysis, phase-contrast microscopy images of microorganisms and microorganisms@*a*MIL-125 (Ti) composites, SEM image of the as-prepared MIL-125 (Ti), zeta potential values of yeast, PCC 6803, *E. coli*, MIL-125 (Ti), yeast@*a*MIL-125 (Ti), PCC 6803@*a*MIL-125 (Ti), and *E. coli*@*a*MIL-125 (Ti) composites in water, FTIR spectra of yeast and yeast@*a*MIL-125 (Ti) composites, XPS characterization of yeast and yeast@*a*MIL-125 (Ti) composites, effects of pH on the adsorption of glyphosate by yeast@*a*MIL-125 (Ti) composites, FTIR and XPS characterization of yeast@*a*MIL-125 (Ti) composites and yeast@aMIL-125 (Ti)@glyphosate, N_2 adsorption−desorption isotherms of yeast@*a*MIL-125 (Ti) composites before and after glyphosate adsorption, the supernatants of glyphosate adsorbed by yeast@aMIL-125 and yeast and the UV−visible adsorption spectrum of *N*-nitroso-glyphosate generated from the solution, effect of coexisting cations on the adsorption of glyphosate by yeast@*a*MIL-125 (Ti) composites, and reusability of microorganisms@*a*MIL-125 (Ti) composites (PDF)

■ AUTHOR INFORMATION

Corresponding Authors

Mingshun Li − *State Key Laboratory of Agricultural Microbiology and College of Life Science and Technology, Huazhong Agricultural University, Wuhan 430070, China; Hubei Hongshan Laboratory, Wuhan 430070, China*; Email: mshli7125@mail.hzau.edu.cn

Yonggang Hu − *State Key Laboratory of Agricultural Microbiology and College of Life Science and Technology, Huazhong Agricultural University, Wuhan 430070, China; Hubei Hongshan Laboratory, Wuhan 430070, China*; orcid.org/0000-0002-3337-4223; Email: yongganghu@mail.hzau.edu.cn

Authors

Yuqiang Xiang − *State Key Laboratory of Agricultural Microbiology and College of Life Science and Technology, Huazhong Agricultural University, Wuhan 430070, China; Hubei Hongshan Laboratory, Wuhan 430070, China; College of Veterinary Medicine, Henan Agricultural University, Zhengzhou 450002, China*

Huaduo Yan − *College of Food and Biological Engineering, Henan University of Animal Husbandry and Economy, Zhengzhou 450000, China*

Fei Peng − *State Key Laboratory of Agricultural Microbiology and College of Life Science and Technology, Huazhong Agricultural University, Wuhan 430070, China; Hubei Hongshan Laboratory, Wuhan 430070, China*; orcid.org/0000-0001-6542-2130

Weikang Ke − *State Key Laboratory of Agricultural Microbiology and College of Life Science and Technology, Huazhong Agricultural University, Wuhan 430070, China; Hubei Hongshan Laboratory, Wuhan 430070, China*

Aroosha Faheem − *State Key Laboratory of Agricultural Microbiology and College of Life Science and Technology, Huazhong Agricultural University, Wuhan 430070, China; Hubei Hongshan Laboratory, Wuhan 430070, China*

Complete contact information is available at: https://pubs.acs.org/10.1021/acsomega.2c06329

Author Contributions

The manuscript was written through contributions of all authors. All authors have given approval to the final version of the manuscript. Y.X., H.Y., and F.P. contributed equally to this work.

Notes

The authors declare no competing financial interest.

■ ACKNOWLEDGMENTS

This work was supported by the National Natural Science Foundation of China (grant nos. 21675057 and 31970095), the National Key Research and Development Program of China (grant nos. 2018YFE0105600 and 2016YFD0500900), the Fundamental Research Funds for the Central Universities (grant no. 2662018PY054), the China Postdoctoral Science Foundation (grant nos. 2021M690927 and 2022T150196), the National Natural Science Foundation of China (grant no. 32100085), and the Key R&D and Promotion in Henan Province Special Project (grant no. 212102110224 and 222102110036).

REFERENCES

(1) Bennett, T. D.; Horike, S. Liquid, glass and amorphous solid states of coordination polymers and metal−organic frameworks. *Nat. Rev. Mater.* **2018**, *3*, 431−440.

(2) Li, J.; Huang, W.; Wang, M.; Xi, S.; Meng, J.; Zhao, K.; Jin, J.; Xu, W.; Wang, Z.; Liu, X.; et al. Low-Crystalline Bimetallic Metal−Organic Framework Electrocatalysts with Rich Active Sites for Oxygen Evolution. *ACS Energy Lett.* **2019**, *4*, 285−292.

(3) Gao, Y.; Deng, S. Q.; Jin, X.; Cai, S. L.; Zheng, S.-R.; Zhang, W. G. The construction of amorphous metal-organic cage-based solid for rapid dye adsorption and time-dependent dye separation from water. *Chem. Eng. J.* **2019**, *357*, 129−139.

(4) Zhang, X.; Li, G.; Zhang, Y.; Luo, D.; Yu, A.; Wang, X.; Chen, Z. Amorphizing metal-organic framework towards multifunctional polysulfide barrier for high-performance lithium-sulfur batteries. *Nano Energy* **2021**, *86*, No. 106094.

(5) Orellana-Tavra, C.; Baxter, E. F.; Tian, T.; Bennett, T. D.; Slater, N. K. H.; Cheetham, A. K.; Fairen-Jimenez, D. Amorphous metal−organic frameworks for drug delivery. *Chem. Commun.* **2015**, *51*, 13878−13881.

(6) Zhou, H.; Zheng, M.; Tang, H.; Xu, B.; Tang, Y.; Pang, H. Amorphous Intermediate Derivative from ZIF-67 and Its Outstanding Electrocatalytic Activity. *Small* **2020**, *16*, No. 1904252.

(7) Liu, C.; Wang, J.; Wan, J.; Cheng, Y.; Huang, R.; Zhang, C.; Hu, W.; Wei, G.; Yu, C. Amorphous Metal-Organic Framework-Dominated Nanocomposites with Both Compositional and Structural Heterogeneity for Oxygen Evolution. *Angew. Chem., Int. Ed.* **2020**, *59*, 3630−3637.

(8) Zhang, T.; Wang, J.; Zhang, W.; Yang, C.; Zhang, L.; Zhu, W.; Sun, J.; Li, G.; Li, T.; Wang, J. Amorphous Fe/Mn bimetal−organic frameworks: outer and inner structural designs for efficient arsenic(iii) removal. *J. Mater. Chem. A* **2019**, *7*, 2845−2854.

(9) Fonseca, J.; Choi, S. Synthesis of a novel amorphous metal organic framework with hierarchical porosity for adsorptive gas separation. *Microporous Mesoporous Mater.* **2021**, *310*, No. 110600.

(10) Jin, X.; Zhang, Y. P.; Li, D. M.; Ma, D.; Zheng, S. R.; Wu, C. H.; Li, J. Y.; Zhang, W. G. The interaction of an amorphous metal-organic cage-based solid (aMOC) with miRNA/DNA and its application on a quartz crystal microbalance (QCM) sensor. *Chem. Commun.* **2020**, *56*, 591−594.

(11) Wu, X.; Yue, H.; Zhang, Y.; Gao, X.; Li, X.; Wang, L.; Cao, Y.; Hou, M.; An, H.; Zhang, L.; et al. Packaging and delivering enzymes by amorphous metal-organic frameworks. *Nat. Commun.* **2019**, *10*, 5165.

(12) Conrad, S.; Kumar, P.; Xue, F.; Ren, L.; Henning, S.; Xiao, C.; Mkhoyan, K. A.; Tsapatsis, M. Controlling Dissolution and Transformation of Zeolitic Imidazolate Frameworks by using Electron-Beam-Induced Amorphization. *Angew. Chem., Int. Ed.* **2018**, *57*, 13592−13597.

(13) Chapman, K. W.; Halder, G. J.; Chupas, P. J. Pressure-induced amorphization and porosity modification in a metal-organic framework. *J. Am. Chem. Soc.* **2009**, *131*, 17546−17547.

(14) Hu, Y.; Kazemian, H.; Rohani, S.; Huang, Y.; Song, Y. In situ high pressure study of ZIF-8 by FTIR spectroscopy. *Chem. Commun.* **2011**, *47*, 12694−12696.

(15) Graham, A. J.; Banu, A.-M.; Düren, T.; Greenaway, A.; McKellar, S. C.; Mowat, J. P. S.; Ward, K.; Wright, P. A.; Moggach, S. A. Stabilization of Scandium Terephthalate MOFs against Reversible Amorphization and Structural Phase Transition by Guest Uptake at Extreme Pressure. *J. Am. Chem. Soc.* **2014**, *136*, 8606−8613.

(16) Su, Z.; Miao, Y.-R.; Mao, S.-M.; Zhang, G.-H.; Dillon, S.; Miller, J. T.; Suslick, K. S. Compression-Induced Deformation of Individual Metal−Organic Framework Microcrystals. *J. Am. Chem. Soc.* **2015**, *137*, 1750−1753.

(17) Cao, S.; Bennett, T. D.; Keen, D. A.; Goodwin, A. L.; Cheetham, A. K. Amorphization of the prototypical zeolitic imidazolate framework ZIF-8 by ball-milling. *Chem. Commun.* **2012**, *48*, 7805−7807.

(18) Bennett, T. D.; Cao, S.; Tan, J. C.; Keen, D. A.; Bithell, E. G.; Beldon, P. J.; Friscic, T.; Cheetham, A. K. Facile Mechanosynthesis of Amorphous Zeolitic Imidazolate Frameworks. *J. Am. Chem. Soc.* **2011**, *133*, 14546−14549.

(19) Bennett, T. D.; Keen, D. A.; Tan, J.-C.; Barney, E. R.; Goodwin, A. L.; Cheetham, A. K. Thermal Amorphization of Zeolitic Imidazolate Frameworks. *Angew. Chem., Int. Ed.* **2011**, *50*, 3067−3071.

(20) Martí-Rujas, J.; Islam, N.; Hashizume, D.; Izumi, F.; Fujita, M.; Kawano, M. Dramatic Structural Rearrangements in Porous Coordination Networks. *J. Am. Chem. Soc.* **2011**, *133*, 5853−5860.

(21) Zhang, X.; Song, L.; Bi, F.; Zhang, D.; Wang, Y.; Cui, L. Catalytic oxidation of toluene using a facile synthesized Ag nanoparticle supported on UiO-66 derivative. *J. Colloid Interface Sci.* **2020**, *571*, 38−47.

(22) Moghadam, P. Z.; Li, A.; Liu, X.-W.; Bueno-Perez, R.; Wang, S.-D.; Wiggin, S. B.; Wood, P. A.; Fairen-Jimenez, D. Targeted classification of metal−organic frameworks in the Cambridge structural database (CSD). *Chem. Sci.* **2020**, *11*, 8373−8387.

(23) Xiang, Y.; Zhang, Y.; Sun, X.; Chai, Y.; Xu, X.; Hu, Y. Rapid Self-Assembly of Au Nanoparticles on Rigid Mesoporous Yeast-Based Microspheres for Sensitive Immunoassay. *ACS Appl. Mater. Interfaces* **2018**, *10*, 43450−43461.

(24) Xiang, Y.; Yan, H.; Zheng, B.; Faheem, A.; Hu, Y. Microorganism@UiO-66-NH_2 Composites for the Detection of Multiple Colorectal Cancer-Related microRNAs with Flow Cytometry. *Anal. Chem.* **2020**, *92*, 12338−12346.

(25) Xiang, Y.; Yan, H.; Zheng, B.; Faheem, A.; Chen, W.; Hu, Y. *E. coli*@UiO-67 composites as a recyclable adsorbent for bisphenol A removal. *Chemosphere* **2021**, *270*, No. 128672.

(26) Xiang, Y.; Yan, H.; Zheng, B.; Faheem, A.; Guo, A.; Hu, C.; Hu, Y. Light-Regulated Natural Fluorescence of the PCC 6803@ZIF-8 Composite as an Encoded Microsphere for the Detection of Multiple Biomarkers. *ACS Sens.* **2021**, *6*, 2574−2583.

(27) Shen, S.; Zhou, R.; Li, Y.; Liu, B.; Pan, G.; Liu, Q.; Xiong, Q.; Wang, X.; Xia, X.; Tu, J. Bacterium, Fungus, and Virus Microorganisms for Energy Storage and Conversion. *Small Methods* **2019**, *3*, No. 1900596.

(28) Fan, J. X.; Peng, M. Y.; Wang, H.; Zheng, H. R.; Liu, Z. L.; Li, C. X.; Wang, X. N.; Liu, X. H.; Cheng, S. X.; Zhang, X. Z. Engineered Bacterial Bioreactor for Tumor Therapy via Fenton-Like Reaction with Localized H_2O_2 Generation. *Adv. Mater.* **2019**, *31*, No. e1808278.

(29) Zhang, S.; Li, H.; Wang, S.; Liu, Y.; Chen, H.; Lu, Z. X. Bacteria-Assisted Synthesis of Nanosheet-Assembled TiO_2 Hierarchical Architectures for Constructing TiO_2-Based Composites for Photocatalytic and Electrocatalytic Applications. *ACS Appl. Mater. Interfaces* **2019**, *11*, 37004−37012.

(30) Liu, L.; Zhao, J.; Yin, W.; Lv, S.; Su, M.; Li, P.; Zheng, X.; Chiang, P.; Wu, J. Enhanced immobilization of Cr(VI) by a Fe^0−microorganisms composite system: Benchmark and pot experiments. *J. Environ. Qual.* **2021**, *50*, 1123−1134.

(31) Fatima, R.; Park, S.; Kim, J.-O. Effect of molar ration of Ti/Ligand on the synthesis of MIL-125(Ti) and its adsorption and photocatalytic properties. *J. Ind. Eng. Chem.* **2020**, *90*, 166−177.

(32) Bennett, T. D.; Cheetham, A. K. Amorphous metal-organic frameworks. *Acc. Chem. Res.* **2014**, *47*, 1555−1562.

(33) Fei, R.-H.; Tan, C.; Huang, Y.; Chen, H.-C.; Guo, A.-Z.; Wang, H.-L.; Hu, Y.-G. Self-Assembled Ti^{4+}@Biospore Microspheres for Sensitive DNA Analysis. *ACS Appl. Mater. Interfaces* **2017**, *9*, 34696−34705.

(34) Hemalatha, K.; Prakash, A. S.; Guruprakash, K.; Jayakumar, M. TiO_2 coated carbon nanotubes for electrochemical energy storage. *J. Mater. Chem. A* **2014**, *2*, 1757−1766.

(35) Zhao, M.; Deng, K.; He, L.; Liu, Y.; Li, G.; Zhao, H.; Tang, Z. Core−Shell Palladium Nanoparticle@Metal−Organic Frameworks as Multifunctional Catalysts for Cascade Reactions. *J. Am. Chem. Soc.* **2014**, *136*, 1738−1741.

https://doi.org/10.1021/acsomega.2c06329
ACS Omega 2023, 8, 2164−2172

(36) Liu, M.; Ding, X.; Yang, Q.; Wang, Y.; Zhao, G.; Yang, N. A pM leveled photoelectrochemical sensor for microcystin-LR based on surface molecularly imprinted TiO_2@CNTs nanostructure. *J. Hazard. Mater.* **2017**, *331*, 309−320.
(37) Jindal, A.; Tashiro, K.; Kotani, H.; Takei, T.; Reichenberger, S.; Marzun, G.; Barcikowski, S.; Kojima, T.; Yamamoto, Y. Excellent Oxygen Reduction Reaction Performance in Self-Assembled Amyloid-β/Platinum Nanoparticle Hybrids with Effective Platinum−Nitrogen Bond Formation. *ACS Appl. Energy Mater.* **2019**, *2*, 6536−6541.
(38) Qin, D.; Liu, Z.; Zhao, Y.; Xu, G.; Zhang, F.; Zhang, X. A sustainable route from corn stalks to N, P-dual doping carbon sheets toward high performance sodium-ion batteries anode. *Carbon* **2018**, *130*, 664−671.
(39) Sánchez-Sánchez, A.; Suárez-García, F.; Martínez-Alonso, A.; Tascón, J. M. D. Evolution of the complex surface chemistry in mesoporous carbons obtained from polyaramide precursors. *Appl. Surf. Sci.* **2014**, *299*, 19−28.
(40) Wu, Y. M.; Liu, J. Q.; Cao, H. T.; Wu, Z. Y.; Wang, Q.; Ma, Y. P.; Jiang, H.; Wen, F.; Pei, Y. T. On the adhesion and wear resistance of DLC films deposited on nitrile butadiene rubber: A Ti-C interlayer. *Diamond Relat. Mater.* **2020**, *101*, No. 107563.
(41) Zong, H.; Yu, K.; Zhu, Z. Heterostructure nanohybrids of Ni-doped $MoSe_2$ coupled with Ti_2NT_x toward efficient overall water splitting. *Electrochim. Acta* **2020**, *353*, No. 136598.
(42) Hong, X.; Peng, Y.; Bai, J.; Ning, B.; Liu, Y.; Zhou, Z.; Gao, Z. A novel opal closest-packing photonic crystal for naked-eye glucose detection. *Small* **2014**, *10*, 1308−1313.
(43) Zong, H.; Qi, R.; Yu, K.; Zhu, Z. Ultrathin Ti_2NTx MXene-wrapped MOF-derived CoP frameworks towards hydrogen evolution and water oxidation. *Electrochim. Acta* **2021**, *393*, No. 139068.
(44) Li, J.; Wang, Y.; Yu, Y.; Li, Q. Functionality proportion and corresponding stability study of multivariate metal-organic frameworks. *Chin. Chem. Lett.* **2018**, *29*, 837−841.
(45) Fonseca, J.; Gong, T.; Jiao, L.; Jiang, H.-L. Metal−organic frameworks (MOFs) beyond crystallinity: amorphous MOFs, MOF liquids and MOF glasses. *J. Mater. Chem. A* **2021**, *9*, 10562−10611.
(46) De Yoreo, J. J.; Vekilov, P. G. Principles of Crystal Nucleation and Growth. *Rev. Mineral. Geochem.* **2003**, *54*, 57−93.
(47) Duke, S. O.; Powles, S. B. Glyphosate: a once-in-a-century herbicide. *Pest Manage. Sci.* **2008**, *64*, 319−325.
(48) Bai, S. H.; Ogbourne, S. M. Glyphosate: environmental contamination, toxicity and potential risks to human health via food contamination. *Environ. Sci. Pollut. Res.* **2016**, *23*, 18988−19001.
(49) Valle, A. L.; Mello, F. C. C.; Alves-Balvedi, R. P.; Rodrigues, L. P.; Goulart, L. R. Glyphosate detection: methods, needs and challenges. *Environ. Chem. Lett.* **2018**, *17*, 291−317.
(50) Munoz, J. P.; Bleak, T. C.; Calaf, G. M. Glyphosate and the key characteristics of an endocrine disruptor: A review. *Chemosphere* **2020**, *270*, No. 128619.
(51) Milojević-Rakić, M.; Janošević, A.; Krstić, J.; Nedić Vasiljević, B.; Dondur, V.; Ćirić-Marjanović, G. Polyaniline and its composites with zeolite ZSM-5 for efficient removal of glyphosate from aqueous solution. *Microporous Mesoporous Mater.* **2013**, *180*, 141−155.
(52) Ueda Yamaguchi, N.; Bergamasco, R.; Hamoudi, S. Magnetic $MnFe_2O_4$−graphene hybrid composite for efficient removal of glyphosate from water. *Chem. Eng. J.* **2016**, *295*, 391−402.
(53) Li, Y.; Zhao, C.; Wen, Y.; Wang, Y.; Yang, Y. Adsorption performance and mechanism of magnetic reduced graphene oxide in glyphosate contaminated water. *Environ. Sci. Pollut. Res.* **2018**, *25*, 21036−21048.
(54) Jiang, X.; Ouyang, Z.; Zhang, Z.; Yang, C.; Li, X.; Dang, Z.; Wu, P. Mechanism of glyphosate removal by biochar supported nano-zero-valent iron in aqueous solutions. *Colloids Surf., A* **2018**, *547*, 64−72.
(55) Guo, F.; Zhou, M.; Xu, J.; Fein, J. B.; Yu, Q.; Wang, Y.; Huang, Q.; Rong, X. Glyphosate adsorption onto kaolinite and kaolinite-humic acid composites: Experimental and molecular dynamics studies. *Chemosphere* **2021**, *263*, No. 127979.
(56) Zhu, X.; Li, B.; Yang, J.; Li, Y.; Zhao, W.; Shi, J.; Gu, J. Effective adsorption and enhanced removal of organophosphorus pesticides from aqueous solution by Zr-based MOFs of UiO-67. *ACS Appl. Mater. Interfaces* **2015**, *7*, 223−231.
(57) Yang, Q.; Wang, J.; Zhang, W.; Liu, F.; Yue, X.; Liu, Y.; Yang, M.; Li, Z.; Wang, J. Interface engineering of metal organic framework on graphene oxide with enhanced adsorption capacity for organo-phosphorus pesticide. *Chem. Eng. J.* **2017**, *313*, 19−26.
(58) Ho, Y. S.; McKay, G. Pseudo-second order model for sorption processes. *Process Biochem.* **1999**, *34*, 451−465.
(59) Ho, Y. S.; McKay, G. The kinetics of sorption of divalent metal ions onto sphagnum moss peat. *Water Res.* **2000**, *34*, 735−742.
(60) Yang, Q.; Wang, J.; Chen, X.; Yang, W.; Pei, H.; Hu, N.; Li, Z.; Suo, Y.; Li, T.; Wang, J. The simultaneous detection and removal of organophosphorus pesticides by a novel Zr-MOF based smart adsorbent. *J. Mater. Chem. A* **2018**, *6*, 2184−2192.
(61) Phatthanakittiphong, T.; Seo, G. T. Characteristic Evaluation of Graphene Oxide for Bisphenol A Adsorption in Aqueous Solution. *Nanomaterials* **2016**, *6*, 128.
(62) Wei, K.; Wang, X.; Jiao, X.; Li, C.; Chen, D. Self-supported three-dimensional macroporous amorphous NiFe bimetallic-organic frameworks for enhanced water oxidation. *Appl. Surf. Sci.* **2021**, *550*, No. 149323.
(63) Li, C.; Li, Y.; Li, Q.; Duan, J.; Hou, J.; Hou, Q.; Ai, S.; Li, H.; Yang, Y. Regenerable magnetic aminated lignin/Fe_3O_4/$La(OH)_3$ adsorbents for the effective removal of phosphate and glyphosate. *Sci. Total Environ.* **2021**, *788*, No. 147812.
(64) Zavareh, S.; Farrokhzad, Z.; Darvishi, F. Modification of zeolite 4A for use as an adsorbent for glyphosate and as an antibacterial agent for water. *Ecotoxicol. Environ. Saf.* **2018**, *155*, 1−8.
(65) Chen, Q.; Zheng, J.; Yang, Q.; Dang, Z.; Zhang, L. Insights into the Glyphosate Adsorption Behavior and Mechanism by a $MnFe_2O_4$@Cellulose-Activated Carbon Magnetic Hybrid. *ACS Appl. Mater. Interfaces* **2019**, *11*, 15478−15488.
(66) Feng, D.; Xia, Y. Comparisons of glyphosate adsorption properties of different functional Cr-based metal−organic frameworks. *J. Sep. Sci.* **2018**, *41*, 732−739.
(67) Xie, Q.; Li, Y.; Lv, Z.; Zhou, H.; Yang, X.; Chen, J.; Guo, H. Effective Adsorption and Removal of Phosphate from Aqueous Solutions and Eutrophic Water by Fe-based MOFs of MIL-101. *Sci. Rep.* **2017**, *7*, 3316.
(68) Li, Y.; Xie, Q.; Hu, Q.; Li, C.; Huang, Z.; Yang, X.; Guo, H. Surface modification of hollow magnetic Fe_3O_4@NH_2-MIL-101(Fe) derived from metal-organic frameworks for enhanced selective removal of phosphates from aqueous solution. *Sci. Rep.* **2016**, *6*, 30651.

https://doi.org/10.1021/acsomega.2c06329
ACS Omega 2023, 8, 2164−2172